

Bathtub vortex in superfluid ^4He

Sosuke Inui,¹ Tomo Nakagawa,¹ and Makoto Tsubota²

¹*Department of Physics, Osaka City University, 3-3-138 Sugimoto, 558-8585 Osaka, Japan*

²*Department of Physics & Nambu Yoichiro Institute of Theoretical and Experimental Physics (NITEP) & The OCU Advanced Research Institute for Natural Science and Technology (OCARINA), Osaka City University, 3-3-138 Sugimoto, 558-8585 Osaka, Japan*

(Dated: December 22, 2024)

We have investigated the structure of macroscopic suction flows in superfluid ^4He . In this study, we primarily analyze the structure of the quantized vortex bundle that appears to play an important role in such systems. Our study is motivated by a series of recent experiments conducted by a research group in Osaka City University [Yano *et al.*, J. Phys. Conf. Ser. **969**, 012002 (2018)]; they created a suction vortex using a rotor in superfluid ^4He . They also reported that up to 10^4 quantized vortices accumulated in the central region of the rotating flow. The quantized vortices in such macroscopic flows are assumed to form a bundle structure; however, the mechanism has not yet been fully investigated. Therefore, we prescribe a macroscopic suction flow to the normal fluid and discuss the evolution of a giant vortex (*i.e.*, one with a circulation quantum number exceeding unity) and a bundle of singly quantized vortices from a small number of seed vortices. Then, using numerical simulations, we discuss several possible characteristic structures of the bundle in such a flow, and we suggest that the actual steady-state bundle structure in the experiment can be verified by measuring the diffusion constant of the vortex bundle after the macroscopic normal flow has been switched off. By applying extensive knowledge of the superfluid ^4He system, we elucidate a new type of macroscopic superfluid flow and identify a novel structure of quantized vortices.

I. INTRODUCTION

We often encounter “vortices” of various length scales: the dropping of milk into coffee, whirlpools, the Great Red Spot on the surface of Jupiter, and so on. The suction vortex, also referred to as the “bathtub vortex,” is one of the most familiar classical vortices; it can be easily produced by unplugging a bathtub filled with water. However, this vortex’s simple generation procedure does not entail that its structure can be easily understood. Indeed, despite several attempts, no theory of the vortex has yet been completed [1–3]. In this paper, we elucidate the bathtub vortex from a different perspective: that of a bathtub vortex in superfluid ^4He .

Liquid ^4He , at a saturated evaporation pressure below the lambda point $T_\lambda \approx 2.17$ K, exhibits superfluidity; in this state, its shear viscosity vanishes and a number of eccentric phenomena (e.g., fountain and capillary effects) can be observed. These effects are often explained using a phenomenological model (the so-called “two-fluid model” [4–6]), in which the superfluid ^4He at $0 < T < T_\lambda$ features two fluid components: an inviscid superfluid with density $\rho_s(T)$ and a viscous normal-fluid with density $\rho_n(T)$. One of the most notable properties of superfluids is that their circulation $\kappa \equiv \oint_{\mathcal{L}} \mathbf{v} \cdot d\mathbf{l}$ can be quantized as

$$\kappa = \frac{h}{m}n, \quad (1)$$

where n is an integer, h is Planck’s constant, and m is the mass of a ^4He atom. This quantization assumes that the path \mathcal{L} encloses a filamentary topological defect in the superfluid. The topological defects with a quantized circulation always form closed loops or terminate their ends at boundaries, and thus they are called quantized vortex

loops or lines [7]. In a bulk superfluid, the kinetic energy per unit length of the vortex line ϵ is proportional to n^2 ; thus, it is more energetically stable to have two vortices with $n = 1$ than one vortex with $n = 2$. The superfluid system is very clean and offers an ideal experimental environment for many fields of physics; thus, it has been extensively studied over the decades by researchers hoping to understand various physical phenomena, including turbulence [8–11], the Kibble–Zurek mechanism [12–14], and pulsar glitches in neutron stars [15, 16].

In the experiments conducted by a research group at Osaka City University (OCU), Yano *et al.* created a macroscopic bathtub vortex by sucking superfluid ^4He (temperature: $T = 1.6$ K) out of a cylindrical container via a drain hole at the bottom, using a rotor (see the schematic overview in Fig. 1 and the figures given in Refs. [17, 18]). The rotor rotated below the drain hole and induced a pressure difference; this allowed normal- and super-fluids to flow. When the fluid achieved a steady state, it mimicked the flow of a classical fluid [17] (as it does under steady solid-body rotation), by forming a vortex lattice [19–24]. The normal fluid has a viscosity; thus, it can be reasonably assumed that its steady-state flow profile resembles the profile discussed in Refs. [1, 2]; that is, the down-flow is narrowly confined in the central region, forming a flow tube above the drain hole. It is classically understood that an up-flow surrounds the down-flow, owing to the vorticity generated near the central region [2]. However, the vorticity of the superfluid is only carried by quantized vortices; therefore, this might not apply in the non-classical case, and the formation of classical-like macroscopic suction flows is not trivial. Moreover, from observations of second sound attenuation, the vortex line density L_L at the core region (radius

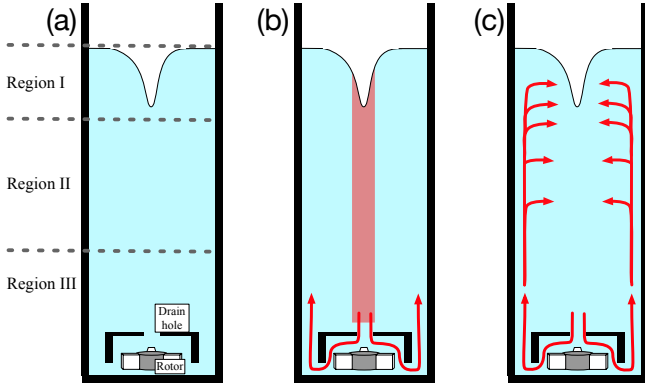


FIG. 1. (a) – Schematic overview of the “bathtub vortex” [17, 18]. The entire length scale of the system (from the surface to the bottom of the fluid) is approximately 20–30 cm. The system can be roughly separated into three regions: Region I, in which the surface of the superfluid ^4He dimples and a large vortex with circulation quantum number $n > 1$ is expected; Region II, in which a steady vortex bundle is thought to develop; and Region III, in which the geometry of the bundle experiences the effects of the bottom boundary. In classical theory, it is understood that an Ekman boundary layer exists at the bottom and an up-flow operates just outside the down-flow travelling through the drain hole. (b) – Expected normal flow pattern. The rotor repels the fluid and generates a pressure difference. Then, the fluid is forced to flow through the drain hole. The classical theory implies that the down-flow of the normal fluid is tightly confined in the central (shaded) region. (c) – Expected trajectory of (remnant) quantized vortices. For the system to have a giant vortex, it must be provided with vortices/vorticity externally; otherwise, it does not conserve angular momentum.

~ 2 mm) is reported to be as much as $1.3 \times 10^{12} \text{ m}^{-2}$ [18]. These vortex lines are thought to be attracted toward the axis of rotation, thereby forming a vortex bundle [25] through the particular macroscopic flow geometry of the bathtub vortex and the flow of the normal fluid, which arises through the mutual friction between the two fluids. Because of this extremely high vortex line density, a full numerical simulation (from a stationary to steady rotating state) is not feasible. Therefore, we consider only the initial evolving state (which is essential to the whole process) and discuss the possible structures of a fully developed vortex bundle in a bathtub vortex. Throughout this analysis, we prescribe the profile of the normal fluid velocity, which is valid only for a short period before the vortex bundle fully develops. The deformation of the normal flow profile is beyond the scope of this study and will be considered in future works.

The generation mechanism of a macroscopic bathtub vortex in a superfluid is not trivial. To understand such novel macroscopic flows in superfluid ^4He , it is necessary to construct models that do not contradict the experimental results; for this, we apply extensive background knowledge on superfluidity and computational techniques developed over several decades. The objective of this

study is to qualitatively understand the formation of giant vortices and vortex bundles in macroscopic suction flows, and to discuss the bundles’ structures. We divide the superfluid bathtub vortex into three regions, as shown in Fig. 1. In Sec. II we briefly review the two numerical models used to simulate vortex dynamics: the 2D vortex point model (VPM) and 3D vortex filament model (VFM). In Sec. III, the process of giant vortex production is discussed. Then, we discuss how vortices are transported from Region I to Region II, using VFM simulations. In Sec. IV, we show that, depending on the geometry of the normal fluid flow, two characteristic vortex bundle structures are possible in Region II: a linear-vortex structure and a cylindrical vortex-layer-like structure. In Sec. V, we qualitatively estimate the characteristic diffusion time scale of the vortex bundles. Finally, in Sec. VI, we summarize the overall structure of a bathtub vortex.

II. EQUATION OF MOTION FOR VORTICES

The core radius of a quantized vortex in superfluid ^4He is of the order of \AA , and a vortex segment carries a potential flow of velocity $v_s \propto 1/r$ around it, where r is the radial distance from the vortex core. Thus, quantized vortices are often treated as having a delta-function-like vorticity at position $\mathbf{s}(\xi)$, using the arc length parameterization ξ . Thus, the motion of a quantized vortex obeys the Helmholtz’s theorems and follows the local superfluid flow $\mathbf{v}_s(\xi)$. However, at finite temperatures, the temperature-dependent mutual friction terms α and α' become significant, and the equation of motion is [26]

$$\frac{d\mathbf{s}(\xi, t)}{dt} = \mathbf{v}_s + \alpha \mathbf{s}'(\xi) \times (\mathbf{v}_n - \mathbf{v}_s) - \alpha' \mathbf{s}'(\xi) \times [\mathbf{s}'(\xi) \times (\mathbf{v}_n - \mathbf{v}_s)], \quad (2)$$

where \mathbf{v}_s and \mathbf{v}_n are the velocity fields of super- and normal-fluids, respectively; the prime symbol $'$ denotes the derivative with respect to arc length ξ . In the following subsections, we rewrite Eq. (2) into suitable forms for VPM and VFM calculations.

A. Numerical Method: Vortex Filament Model

First, we consider a 3D vortex line configuration, discretizing it into segments of length $d\xi$. A vortex segment at $\mathbf{s}(\xi)$ tends to move with velocity $\mathbf{v}_s(\mathbf{s}(\xi))$. The term $\mathbf{v}_s(\mathbf{s}(\xi))$ can be decomposed into three contributions: the velocity $\mathbf{v}_{s,0}$, which is induced by all vortices in the system; the velocity $\mathbf{v}_{s,\text{ext}}$, which is imposed externally; and the velocity $\mathbf{v}_{s,b}$, which is induced by the boundaries. The superfluid velocity $\mathbf{v}_{s,0}$ at ξ is obtained by calculat-

ing the following Biot–Savart integral:

$$\mathbf{v}_{s,0}(\xi) = \frac{\kappa}{4\pi} \int_{\mathcal{L}} \frac{\mathbf{s}'(\xi_1) \times (\mathbf{s}(\xi) - \mathbf{s}(\xi_1))}{|\mathbf{s}(\xi) - \mathbf{s}(\xi_1)|^3} d\xi_1 \quad (3)$$

$$= \mathbf{v}_{s,\text{loc}} + \mathbf{v}_{s,\text{non-loc}}.$$

The integral (3) diverges as $\xi_1 \rightarrow \xi$, because we neglect the core radius a of the vortex. Computationally, we avoid the divergence by separating out the local term from the total integration path \mathcal{L} , to obtain $\mathbf{v}_{s,\text{loc}}$ and $\mathbf{v}_{s,\text{non-loc}}$. Applying the local induction approximation, $\mathbf{v}_{s,\text{loc}}$ can be evaluated as $\mathbf{v}_{s,\text{loc}} \approx \beta \mathbf{s}' \times \mathbf{s}''$, where $\beta = (\kappa/4\pi) \ln(R/a)$. To solve Eq. (2) and perform the simulation, the path \mathcal{L} is divided into segments of $\Delta\xi$, and the integration in Eq. (3) is calculated for each segment and at every time step Δt in the fourth-order Runge–Kutta scheme.

B. Numerical Method: Vortex Point Model

In the VPM, we treat vortices as points on a 2-dimensional plane. Letting \mathbf{r}_i represent the position of the i^{th} vortex, the velocity integral in Eq. (3) simply becomes a summation over all the N points (excluding itself) [27]; thus,

$$\mathbf{v}_{s,0}(\mathbf{r}_j) = \frac{1}{2\pi} \sum_{i=1, i \neq j}^N \kappa_i \frac{\hat{\mathbf{z}} \times (\mathbf{r}_j - \mathbf{r}_i)}{|\mathbf{r}_j - \mathbf{r}_i|^2}, \quad (4)$$

where κ_i is the circulation h/m and is denoted with a plus or minus. $\hat{\mathbf{z}}$ is a unit vector in the z -direction. Substituting Eq. (4) into Eq. (2), the equation of motion simplifies to

$$\frac{d\mathbf{r}_j}{dt} = \mathbf{v}_s(\mathbf{r}_j) + \alpha \kappa_i \hat{\mathbf{z}} \times (\mathbf{v}_n - \mathbf{v}_s(\mathbf{r}_i)) - \alpha' (\mathbf{v}_n - \mathbf{v}_s(\mathbf{r}_i)), \quad (5)$$

where \mathbf{v}_s is the sum of three velocity components: $\mathbf{v}_{s,0}$, induced by the point vortices; $\mathbf{v}_{s,\text{ind}}$, imposed by the external environment; and $\mathbf{v}_{s,b}$, induced by the boundaries. Here, we have used the fact that $\mathbf{s}'(\xi) = \pm 1$ in this geometry. Again, the time integral can be solved by adopting the fourth-order Runge–Kutta scheme after calculating the velocity of each vortex point.

Compared with the VFM, the VPM requires considerably fewer computational resources to conduct the simulation, because it avoids computing the Biot–Savart integral in Eq. (3). However, in reality, the situations in which the VPM can be applied are limited; for example, in 3D spaces with a negligibly small height or those featuring straight vortex lines along the z -axis. In the analysis in Sec. IV, we apply the VPM to the system shown in Fig. 5(b), which differs from the conventional systems in which the VPM is applicable.

We assume a cylindrical container aligned along the z -axis and filled with superfluid ^4He at $T = 1.6$ K. For simplicity, we consider a symmetrically rotating flow of

normal fluid along the z -axis; that is, the normal fluid component takes a Rankine-vortex-like velocity profile that depends on radial distance r as

$$\mathbf{v}_n(r, \phi, z) = \begin{pmatrix} 0 \\ \frac{\Gamma_n}{2\pi} \frac{r}{R_0^2} \\ v_z \end{pmatrix} \quad \text{for } r < R_0 \quad (6)$$

$$\mathbf{v}_n(r, \phi, z) = \begin{pmatrix} 0 \\ \frac{\Gamma_n}{2\pi} \frac{1}{r} \\ 0 \end{pmatrix} \quad \text{for } r > R_0, \quad (7)$$

where R_0 is the radius of the down-flow tube (which is the same size as the drain hole at the bottom of the container), and Γ_n is the circulation of the normal fluid. Here, the superfluid contribution from the external and boundary effects are neglected; that is, $\mathbf{v}_{s,\text{ind}} = 0$ and $\mathbf{v}_{s,b} = 0$; hence, the only contribution to the superfluid velocity field is $\mathbf{v}_{s,0}$. As an initial state, we assume concentric vortex rings oriented perpendicular to the z -axis. We take the xz -plane at $y = 0$ (or equivalently, the rz -plane at $\phi = 0$ and $\phi = \pi$ in the cylindrical coordinate system) and apply the VPM. Because the i^{th} vortex ring now has a local curvature $1/r_i$, we add a correction term, which is the local induction approximation term in Eq. (3); that is,

$$\mathbf{v}_s = \mathbf{v}_{s,0} + \mathbf{v}_{s,\text{loc}}. \quad (8)$$

III. GIANT VORTEX AND VORTEX TRANSPORT IN REGION I

The steady bathtub vortex in ^4He features a deep cavity in the central region. The shape of the cavity indicates that the azimuthal velocities of both the super-

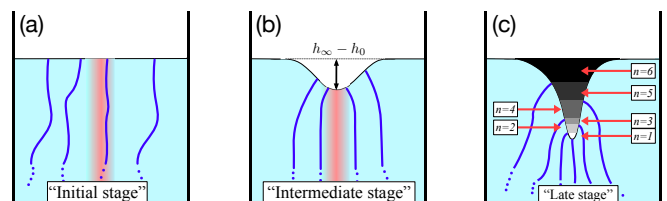


FIG. 2. (a) – (c) Snapshots of the three stages of giant vortex production (color online). The blue lines in each panel represent the singly quantized vortices, and the shaded region around the vertical axis (z -axis) represents the region in which the vorticity of the normal fluid accumulates and forms a strong down-flow. Each stage is briefly described as follows: (a) – Initial stage: vortex lines gather and tend to form a lattice. (b) – Intermediate stage: the surface of the central region dimples owing to the azimuthal velocity, which is inversely proportional to the radial distance r and pressure difference. (c) – Late stage: the dimple grows to become a cavity by “absorbing” singly quantized vortices. At this stage, the normal fluid circulation Γ_n is not necessarily equal to that of the giant vortex, κn_{giant} .

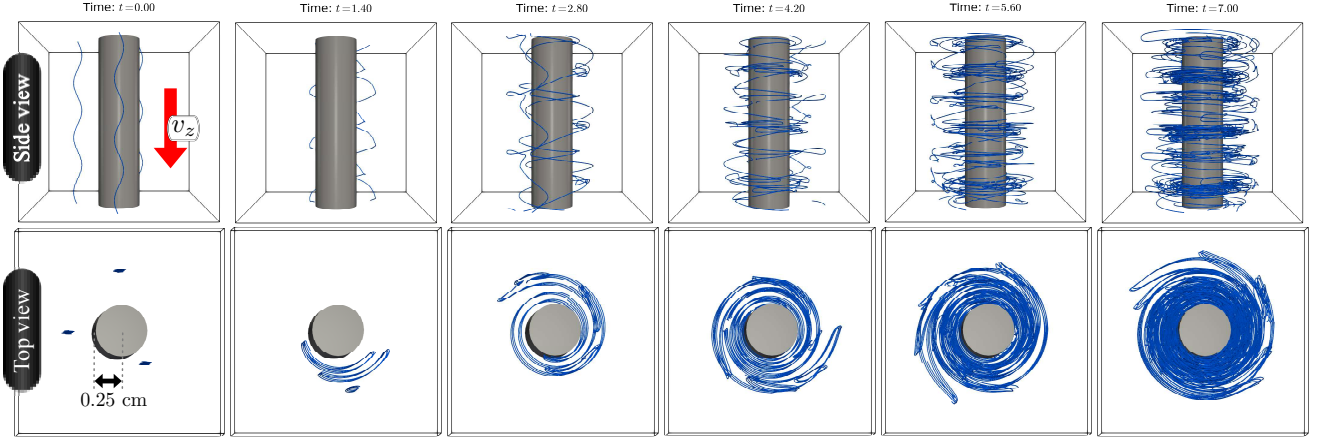


FIG. 3. Series of snapshots of VFM simulation at $t = 0.0, 1.1, 2.2, 3.3, 4.4$, and 5.5 s from left to right, respectively (color online). A box measuring 2 cm in each dimension is drawn for reference. The cylinder (radius: 0.25 cm) in each panel represents a giant vortex, around which the circulation of both fluids are non-zero. In the system, the external normal fluid velocity v_z is applied downward. The top and bottom surfaces of the box are subject to the periodic boundary condition.

and normal-fluids are inversely proportional to the radial distance r around it. This implies that, for a fully developed bathtub vortex, the cavity behaves like a giant vortex; that is, a quantized vortex with a circulation quantum number $n > 1$.

Here, we consider how the giant vortex grows. One of the most conceivable scenarios of giant vortex production in the initial stages of bathtub vortex evolution is as follows: First, the vorticity of the normal fluid accumulates in the central region along the z -axis, and the quantized vortices are also transported toward the central region from the surrounding bulk fluid. As these gather, they start to exhibit a collective rotational motion, forming some type of lattice structure; this is analogous to the triangular-lattice formation observed in solid-body rotating superfluid helium [28], BEC [21–24], and superconducting currents [29]. Then, the surface of the superfluid ^4He gradually starts to deform in the central region, due to the pressure difference and down-flow. The surface becomes increasingly deformed and generates a cavity of depth $h_\infty - h_0$ (as measured from the height of the stationary surface h_∞ at $r \rightarrow \infty$) as the vorticity of the normal fluid accumulates and vertical vortices enter the vicinity; we can identify this as a giant vortex of circulation quantum number $n_{\text{giant}} > 1$. Taking the cavity depth h as a function of radial distance r , $h(0) = h_0$ and $\lim_{r \rightarrow \infty} h(r) = h_\infty$; thus, the quantum number n_{giant} at $h(r)$ can be identified as the number of singly quantized vortex lines attached below the surface, as shown in Fig. 2 (c). In a steady state, the macroscopic flow profiles of the super- and normal-fluids coincide with each other, to minimize the mutual friction; this means that the circulation of each fluid around the entire system is equal; that is, $\Gamma_n = \Gamma_s + \kappa N_{\text{vor}}$. Here, $\Gamma_s = \kappa n_{\text{giant}}$ with $\kappa = h/m$, and N_{vor} is the number of freely floating vortex lines.

If the system is ideally clean (*i.e.*, no remnant vortex rings exist), then after a sufficiently long time, $\Gamma_n = \Gamma_s$

and $\kappa N_{\text{vor}} = 0$ are satisfied, because all the singly quantized vortices are “absorbed” into the giant one. However, because of the geometry of the experimental setup, vortex rings can be constantly transported to the central regions from the side, under the macroscopic flow generated by the rotor (see Fig. 1 (c)). We conducted numerical simulations to qualitatively assess the vortex line distributions in the presence of flows proportional to $1/r$; that is, the azimuthal velocity profiles for normal- and super-fluids were $v_n = \Gamma_n/2\pi r$ and $v_s = \Gamma_s/2\pi r$, respectively, for an r outside the giant vortex (radius: 0.25 cm).

We consider the case in which the normal fluid velocity is steady, but the giant vortex of the superfluid is still growing; that is, $\Gamma_n > \Gamma_s$. Figure 3 shows a series of snapshots of the simulation, conducted with the parameters $\Gamma_n = 5.0 \times 10^{-4} \text{ m}^2/\text{s}$ and $\Gamma_s = 4.5 \times 10^{-4} \text{ m}^2/\text{s}$; the prescribed vertical normal velocity component $v_z = -3.0 \text{ mm/s}$ and zero outside and inside the cylinder, respectively. The cylinder drawn in each panel represents the surface of the superfluid ^4He , where the giant vortex (with circulation Γ_s) is assumed to exist. Initially, three vortex lines exhibiting a Kelvin wave excitation are placed around the giant vortex. The vortex lines and giant vortex are aligned mutually parallel, hence they tend to repel each other. However, because $\Gamma_n > \Gamma_s$, the singly quantized vortex lines are pulled toward the cylinder under mutual friction. In the presence of external flows proportional to $1/r$, the vortices are stretched and spiraled in toward the cylindrical surface, as shown in Fig. 3. Locally, the orientation of the vortex line near the wall is almost parallel to that of the wall; eventually, the tip of the vortex reached the surface.

In this simulation, special attention must be paid when handling the reconnection events between the singly quantized vortices and the giant vortex. When a vortex line approaches and hits the surface of the hollow cylinder

of the giant vortex, a reconnection event is highly likely; this is thought to be a crucial mechanism that sustains the growth of the circulation Γ_s when $\Gamma_n > \Gamma_s$. However, the conventional method of managing these events algorithmically [26] may not be valid in this system, because the boundary condition at the surface of the giant vortex is unknown. We can assume that the singly quantized vortex lines must intersect the surface of the giant vortex perpendicularly, so that the superfluid does not flow out of the fluid through the boundary. The perpendicularity of the vortices at the reconnecting points is approximately attained by introducing an “effective friction” to the ends of the vortex lines where they meet the wall of the giant vortex. In the numerical simulation, we simply set the azimuthal and vertical velocity components of the vortex segment to be zero when it enters the cylinder through the wall. The reconnected segments circle around the giant vortex, and the remaining vortex lines are wound around the cylinder; this can be observed in the panels in Fig 4 and in the video found in Ref. [30]. However, in the presence of the vertical normal flow, only the vortex segments whose orientations are such that they induces an increasing superfluid flow along the normal flow grow selectively; meanwhile, those with the opposite orientation tend to diminish gradually through mutual friction, which is similar to the vortex mill discussed by Schwarz in Ref. [31].

Through the processes discussed in this section, quantized vortices with a specific orientation were selectively produced in Region I; they then travelled to Region II. As vortex lines continue to wind around the giant vortex, the value of the circulation Γ_s increases. When the value of Γ_s becomes sufficiently close to that of Γ_n , the giant vortex no longer attracts the free vortices, and the vortices enter a quasi-stable equilibrium state. The vortices steadily produced in Region I can behave as a “vortex bath,” which is essential to bundle formation in Region II; we discuss this in Sec. IV.

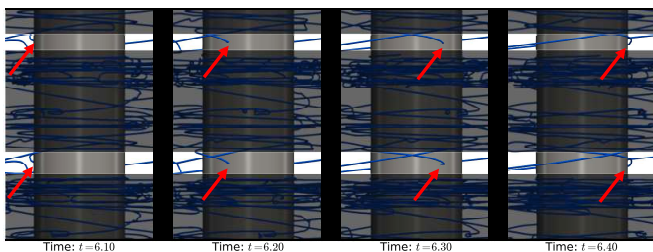


FIG. 4. Series of magnified snapshots of VFM simulation at $t = 6.1, 6.2, 6.3$, and 6.4 s from left to right, respectively (color online). The panels are shaded to render more clearly the growth of the helical structure, which is caused by the motion of the reconnected vortices.

IV. BUNDLE FORMATION IN REGION II

In the presence of a steady down-flow of normal fluid in Region II, several characteristic structural patterns can be found in the vortices densely produced in Region I, provided that the superfluid flow is steady in Region II. For simplicity, the normal fluid velocity profile is assumed to be given by Eqs. (6) and (7), and we neglect the flow profile perturbation attributable to the quantized vortices generated through mutual friction. One factor that characterizes the vortex bundle structure is the ratio of the vertical velocity v_z to the azimuthal velocity v_ϕ of the normal fluid. To observe the effects of this factor, we consider a helical vortex line $\mathbf{s}(\xi)$ with arc length parametrization $\xi \in \mathbb{R}$:

$$\mathbf{s}(\xi) \equiv \begin{pmatrix} x(\xi) \\ y(\xi) \\ z(\xi) \end{pmatrix} = \begin{pmatrix} X_0 \cos k_0 \xi \\ Y_0 \sin k_0 \xi \\ \xi \end{pmatrix}. \quad (9)$$

On the right-hand side of Eq. (2), we neglect all terms except the one proportional to v_n (the second term); then, the equation of motion for $r > R_0$ simplifies to

$$\begin{aligned} \dot{\mathbf{s}}(\xi, t) &\approx \alpha \mathbf{s}' \times \mathbf{v}_n \\ &= A \begin{pmatrix} \left(k_0 v_z \frac{X_0}{Y_0} - \frac{\Gamma_n}{2\pi R_0^2} \right) x \\ \left(k_0 v_z \frac{Y_0}{X_0} - \frac{\Gamma_n}{2\pi R_0^2} \right) y \\ \frac{\Gamma_n k_0}{2\pi R_0^2} \left(\frac{Y_0}{X_0} - \frac{X_0}{Y_0} \right) \end{pmatrix}, \end{aligned} \quad (10)$$

where $A = \alpha / \sqrt{k_0^2(X_0^2 + Y_0^2) + 1}$. When $X_0 = Y_0$, the equation of motion for the helix amplitude $r \equiv \sqrt{x^2 + y^2}$ is simply

$$\dot{r} = \left(k_0 v_z - \frac{\Gamma}{2\pi R_0^2} \right) r. \quad (11)$$

Equation (11) indicates that when $\frac{\Gamma_n}{2\pi R_0^2} > k_0 v_z$, the right-hand side of Eq. (11) becomes negative, and the amplitude r diminishes. Assuming that the maximum wavelength of a vortex line in such a rotating normal fluid tube (radius: R_0) is at most $\lambda_{\max} \equiv 2\pi/k_{0,\min} \sim 2R_0$, then the criterion for the helical excitation on the vortex line to diminish becomes

$$\frac{v_\phi}{v_z} \gtrsim \pi, \quad (12)$$

where $v_\phi \equiv \Gamma_n/2\pi R_0$ is the azimuthal velocity at radial distance $r = R_0$. The validity of the criterion is confirmed through numerical simulations of the VFM in Sec. IV A. Furthermore, we consider the case in which v_z is much greater than v_ϕ in Sec. IV B. We analyze the VPM simulations and discuss our inferences from the computational results.

A. VFM simulations for Region II

We consider the dynamics of six seed vortex rings randomly placed near the central region of radius R_0 ; this is

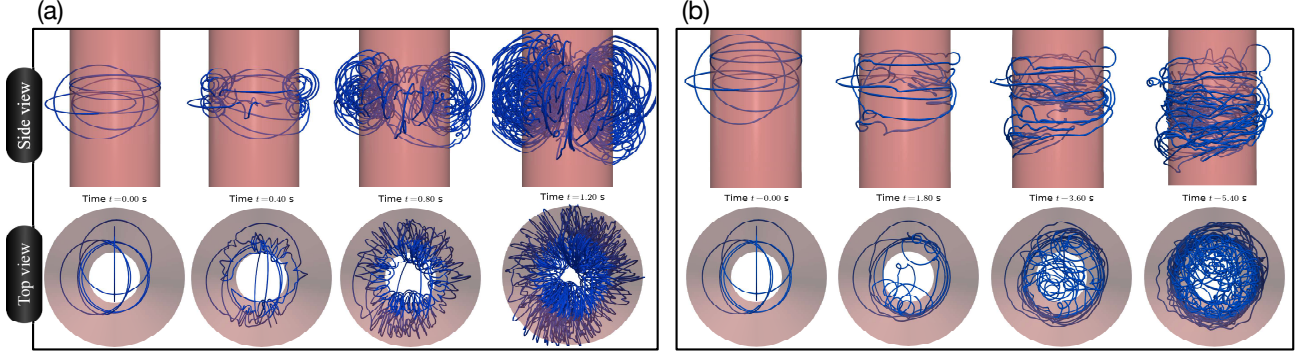


FIG. 5. (a) Snapshots of VFM simulation with $v_z = 10$ mm/s and $v_\phi = 10 \times \pi$ mm/s. The ratio v_z/v_ϕ is chosen to satisfy the relation in Eq. (12). The formation of a bundle of vertical vortex lines can be observed in the central region within the cylindrical shell of radius $R_0 = 2.5$ mm. (b) Snapshots of VFM simulation with $v_z = 10$ mm/s and $v_\phi = 1 \times \pi$ mm/s. Because the relation is not satisfied, the amplitudes of the excitations are significant, and eventually the cylinder of radius R_0 is covered by helical vortex lines.

schematically shown as the shaded region in Fig. 1(b). In numerical simulations, we set the radius $R_0 = 2.5$ mm and $v_z = -10$ mm/s, and we adjust the circulation of normal fluid Γ_n such that $v_\phi = 10 \times \pi$ and $1 \times \pi$ mm/s. Figure 5 (a) and the video in Ref. [32] show the case in which $v_\phi/v_z = \pi$. Small excitations/Kelvin waves in the horizontal direction on the vortex lines are visibly damped, and straight vortex lines tend to align themselves and lengthen in the central region along the z -axis, as the rough estimate in Eq. (12) indicates. However, when the ratio was sufficiently small, the amplitudes of the Kelvin waves are amplified; this can be seen in Fig. 5 (b) and in the video found in Ref. [32]. A helical excitation is amplified in the flow cylinder of radius R_0 . However, when the radius of the excitation exceeds R_0 , it ceases to grow because of the absence of normal flow, which transfers energy through mutual friction. As more helical excitations are generated, vortices are repelled from the central region; these formed a “vortex layer” surrounding the cylinder of radius R_0 . The instability of the vortex layer when the vertical velocity v_z considerably exceeds the azimuthal velocity v_ϕ is discussed in the next subsection, in terms of the VPM simulations.

In both cases, the growth of the vortices along the z -axis appeared to be indefinite while the steady normal flow profile is prescribed; however, in simulations, the maximum vortex line density is limited by the computational resolution $\Delta\xi$. Furthermore, in reality, the dense vortex bundle would significantly deform the normal profile, and our method will eventually break down. We note that our above analysis only applies to the initially growing state of the bundle; however, it is crucial for understanding the structure of the bundle.

B. VPM simulations for Region II

When v_z significantly exceeds v_ϕ , the amplitude of perturbations on the vortex lines is magnified, and a heli-

cal structure develops along the z -axis. By adopting the two-dimensional VPM, we investigated the behaviors of vortex lines in the limit where the tangent vector of the vortices $\mathbf{s}'(\xi)$ lies in the $r\phi$ -plane. In this limit, the only normal fluid component that affects the motion of a vortex point is v_z .

Figure 6 shows the results of a numerical simulation of 2000 point vortices in a system featuring a periodic boundary condition along the z -direction. Here, the vertical normal fluid velocity is $v_z = 4.0$ cm/s for $|x| < R_0 = 0.25$ cm and $v_z = 0$ cm/s elsewhere. The color blue (or red) represents the sign of the circulation, as + (or -); these are placed symmetrically such that the vortices with positive (or negative) signs in the right-hand plane correspond to those with negative (or positive) signs in the left-hand plane after a 180° rotation about the z -axis. A quantitative discussion is not possible using our simulation, because of the lack of detailed knowledge of the actual experimental setup; however, we can infer the following scenario from the qualitative discussion: The point vortices within the region of radius R_0 are pushed toward or away from the axis (depending on their sign) owing to mutual friction; this creates a vortex layer and thereby induces a superfluid velocity field which is aligned parallel to the normal fluid for $|x| < R_0$ and serves to minimize the friction. However, the Kelvin-Helmholtz instability [33–35] becomes significant in the dynamics of this system. As the system evolves, the point vortices tend to form a cluster, or bundle (in 3D). In our numerical model, a point vortex can have a local induced velocity $\mathbf{v}_{s,\text{loc}}$ which is inversely proportional to the radial distance, as described in Sec. II B. Even though the magnitude of the self-induced velocity of an individual point vortex is $v_{\text{one-vor}} \sim \kappa/R_0 \approx 4 \times 10^{-3}$ cm/s, once a cluster of several hundreds or thousands of vortices is formed, the “self-induced velocity of the cluster” v_{cluster} becomes comparable to that of the normal fluid v_z .

The cluster [or bundle (in 3D)] of vortex rings [or helical vortex lines (in 3D)] formed in Region II travel semi-

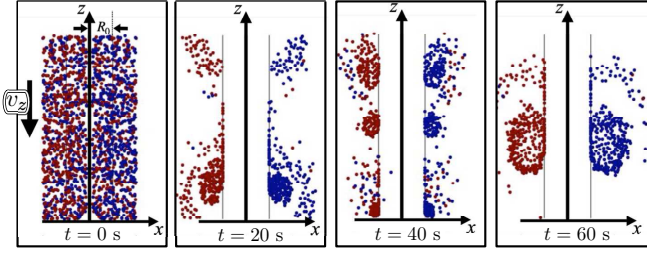


FIG. 6. Snapshots of VPM simulation at $t = 0, 20, 40$, and 60 s from left to right, respectively (color online). A dot represents a point vortex of circulation $\kappa = \pm h/m$. Initially, 1000 point vortices with positive circulations (in blue) and 1000 point vortices with negative circulations (in red) are arranged symmetrically about the z -axis. A vortex point is removed algorithmically once it approaches another point vortex with the opposite sign (within a cut off distance ε), or when it approaches the z -axis (within the distance ε). At $t = 60$ s, a total of 644 point vortices are present, forming a giant dipole vortex pair/vortex ring. See Ref. [36] for a video.

stably if the perturbations in the normal fluid profile remain negligible. Microscopically speaking, this assumption does not hold. Recent studies [37–40] have shown that the normal fluid profile is non-trivially modulated by the presence of quantized vortices, through mutual friction on the scale of the inter-vortex distance. However, in the above analyses, we only considered the macroscopic vortex bundle structure that develops in the macroscopic steady normal flow; a study of the characteristic small-scale structures that emerge due to coupled dynamics remains a future work to be dealt with, and will deepen our knowledge of bathtub vortex systems.

V. ESTIMATION OF DIFFUSION TIME SCALE

The bundle in the steady state is energetically sustained by the normal fluid; thus, when the rotor is stopped, the normal flow slows down and the bundle diffuses. The diffusion constant D of a homogeneous vortex tangle is reported to be of the order of the circulation quantum number $\kappa = h/m$ [41–43]. However, in our case, the bundle is assumed to possess an ordered structure; this would allow the system to have a structure-dependent diffusion constant, which is an experimentally measurable quantity.

We consider a system of N vertical, mutually parallel quantized vortices distributed evenly within a cylindrical region of radius $R_0 = 0.25$ mm. The height of the system is set to 2.0 mm, and the bottom and top surfaces are subject to the periodic boundary condition. The normal fluid component is set to be stationary; thus, the vortices tend to move farther apart from each other through mutual friction. When all the vortices are straight and perpendicular to the z -axis ($n_{\text{twist}} = 0$) (as shown in Fig. 7 (b)), the scenario is relatively simple: The vortices form a triangular lattice as the radius R of the occupied cross-

sectional area grows from its initial value R_0 . Then, the superfluid velocity within the radius R mimics a rigid rotation. However, when the bundle is “twisted” such that all the vortices are helically deformed (as in Fig. 7 (c)), the situation becomes more complex.

First, to qualitatively understand the diffusion process in this system, we consider the kinetic energy E_R of a bundle of N vertical vortex lines confined in a region of radius R . For simplicity, we assume that the vortices are not twisted (*i.e.*, $n_{\text{twist}} = 0$) and that the superfluid velocity profile induced by the vortices is given (in cylindrical polar coordinates) as

$$\mathbf{v}_s(r, \phi, z) = \begin{pmatrix} 0 \\ \frac{\Gamma_s}{2\pi} \frac{r}{R^2} \\ 0 \end{pmatrix} \quad \text{for } r < R, \quad (13)$$

and

$$\mathbf{v}_s(r, \phi, z) = \begin{pmatrix} 0 \\ \frac{\Gamma_s}{2\pi} \frac{1}{r} \\ 0 \end{pmatrix} \quad \text{for } r > R, \quad (14)$$

where $\Gamma_s = \kappa N$. Then, the kinetic energy per unit height can be calculated as $E_R/L_z = (\rho_s/2)2\pi \int_0^{R_{\text{max}}} dr r v_s^2$. Substituting Eqs. (13) and (14) into the integral, the energy is expressed as

$$\frac{E_R}{L_z} = \frac{\Gamma_s^2 \rho_s}{4\pi} \left[\frac{1}{4} + \ln R_{\text{max}} - \ln R \right], \quad (15)$$

where R_{max} is the radius of the cylindrical container. In terms of the area $A \equiv \pi R^2$, the time derivative of Eq. (15) is

$$\frac{d}{dt} \frac{E_R}{L_z} = -\frac{\Gamma_s^2 \rho_s}{8\pi} \frac{\dot{A}}{A}. \quad (16)$$

We can also estimate the energy dissipation rate ε from the mutual friction per unit length between the resting normal fluid and the vortex lines. In the first-order approximation, the frictional force \mathbf{f} per unit length of a vortex segment is known to be proportional to its velocity, and the proportionality constant γ_0 depends on the temperature T [44]. Therefore, we obtain

$$\begin{aligned} \varepsilon &= \mathbf{f} \cdot \mathbf{v}_s \\ &= \frac{\gamma_0 \Gamma_s^2}{4\pi} \sum_{i=1}^N \frac{r_i^2}{R^4} \\ &\approx \frac{\gamma_0 \Gamma_s^2 N}{8\pi A}. \end{aligned} \quad (17)$$

The sum $\sum_{i=1}^N r_i^2$ in the second line is approximately evaluated as $NR^2/2$, assuming an even distribution. The only major factor determining energy loss in the system is the mutual friction; thus, we equate Eq. (16) and Eq. (17) to finally obtain

$$A(t) = A_0 + \frac{\gamma_0 N}{\rho_s} t. \quad (18)$$

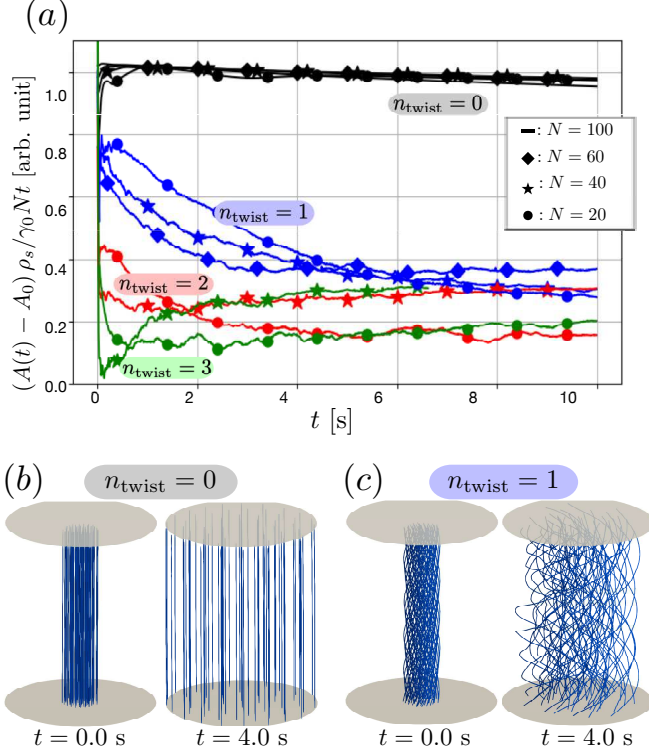


FIG. 7. (a) Normalized cross-sectional areas of the bundles as functions of time for various numbers of vortices N and twists n_{twist} . The values of the functions are proportional to the diffusion constant D . The proportionality constant is found in Eq. (20). (b) – (c) Snapshots of VFM simulations with $N = 60$ vortices for $n_{\text{twist}} = 0$ and 1, respectively. The top and bottom boundaries are subject to the periodic boundary condition. The disks in each panel are of radii 0.8 mm. The video can be found in Ref. [45]

Figure 7 (a) plots the computationally obtained values for the properly normalized areas of the bundle cross-section (*i.e.*, $(A(t) - A_0) \rho_s / \gamma_0 N t$) as functions of time t . It can be clearly seen that when $n = 0$, the values agree with Eq. (18). However, they start to diverge as time elapses; thus, higher-order estimates are needed for a more precise discussion. Interestingly, when $n_{\text{twist}} > 1$, the diffusion of the bundle is strongly suppressed. Although a clear relationship between the number of twists n_{twist} and the reduction in unity in Fig. 7 (a) has not yet been established, the significant suppression of vortex bundle diffusion can be expected in the experiments if the bundle is twisted.

The expression in Eq. (18) relates to the diffusion constant D in conventional 2-dimensional diffusion problems; that is, $\dot{n} = D \nabla^2 n$. A solution to the partial differential equation, using an instantaneous delta function-like source at time $t = 0$, takes the form

$$n(r, t) = \frac{N}{4\pi Dt} \exp\left(-\frac{r^2}{4Dt}\right), \quad (19)$$

where $n(r, t)$ is the vortex number density such that

$N = 2\pi \int_0^\infty r n(r, t) dr$ is the total number of vortices. The radius R of the cross-sectional area of the bundle is characterized by the exponential function in Eq. (19), and $R \sim \sqrt{4Dt}$. Combining this result with Eq. (18), we obtain the final expression:

$$D \approx \frac{\gamma_0 N}{4\pi \rho_s}. \quad (20)$$

In the experiment at OCU, because the temperature T was 1.6 K and the number of vortices N was of order 10^4 , the diffusion constant was approximately $D \approx 8 \text{ mm}^2/\text{s}$. The values of the temperature-dependent quantities γ_0 and ρ_s can be found in Ref. [46].

If we linearly extrapolate our computational results for the simplified system, then the diffusion constant measurable in the experiment is $\sim 2 \text{ mm}^2/\text{s}$ if the vortex bundle is twisted. In our above analysis, the normal fluid is assumed to be at rest for the sake of simplicity; however, in the case of an experiment where 10^4 vortices are present, this assumption may not be valid. If the bundle of vortices and the normal flow co-rotate about the z -axis, then the energy loss via mutual friction in Eq. (17) is reduced; this would lead to further reduction of the diffusion constant.

VI. CONCLUSIONS AND DISCUSSION

Motivated by an experimental report on the “bathtub” vortex of superfluid ^4He , we discussed the structure of the quantized vortex bundle that can be formed in such a macroscopic flow, based on numerical simulations using the VFM and VPM. The superfluid bathtub vortex system was investigated by separating it into three regions. The top region (Region I) is assumed to contain a giant vortex with multiply quantized circulation. By analogy with the rotating superfluid ^4He , we illustrated the giant vortex’s development process. In Region I, a vortex bundle can develop alongside the giant vortex. The bundle that formed around the giant vortex appeared to be a major source of the vortices that were transferred to Region II; thus, it can be considered as a “vortex-line bath.” Region II is the region in which the boundary effect of the vessel bottom is negligible and a vortex-line bath is present. Because the normal fluid has an intrinsic viscosity, we assume that it establishes a macroscopic steady flow. The steady normal flow “stirs” the transferred vortex loops; this presumably deforms the bundle structurally, reflecting the geometry of the normal flow. Then, the bundle settles in a steady state such that the mutual friction between the two fluids is minimized.

The velocity profile of the normal fluid in our analysis is that of a Rankine-vortex-like flow, containing a vertical flow within a radius R_0 along the z -axis, as described in Eqs. (6) and (7). In such environments, the vortices that constitute a bundle either (a) align themselves parallelly along the z -axis or (b) wind around the down-flow region of radius R_0 and form a cylindrical vortex layer. Whether

the bundle takes the structure (a) or (b) depends on the ratio of the vertical velocity v_z to the azimuthal velocity v_ϕ of the normal fluid. Because of the complexity of the experimental setup, no direct experimental data are currently available to indicate size of the ratio. Instead of measuring the ratio, we proposed that the structure could be elucidated indirectly, by measuring the decay of the vortex bundle. In the OCU experiment, the expected vortex diffusion constant D was approximately $8 \text{ mm}^2/\text{s}$, if the bundle was not twisted along the z -axis. A series of VFM simulations indicate that the diffusion constant is significantly reduced if the bundle is twisted. By experimentally measuring the extent to which the diffusion

constant diverges from its expected value, we can further our understanding of the structures of vortex bundles in macroscopic bathtub vortices.

ACKNOWLEDGMENTS

We thank Ken Obara for useful discussions. This work was supported by JSPS KAKENHI Grant No. JP20H01855. S. I. was supported by Grant-in-Aid for JSPS Fellow Grant No. JP20J23131.

-
- [1] T. S. Lundgren, *J. Fluid Mech.* **155**, 381 (1985).
 - [2] A. Andersen, T. Bohr, B. Stenum, J. J. Rasmussen, and B. Lautrup, *J. Fluid Mech.* **556**, 121 (2006).
 - [3] S. Mulligan, G. De Cesare, J. Casserly, and R. Sherlock, *Sci. Rep.* **8**, 824 (2018).
 - [4] L. Tisza, *Nature* **141**, 913 (1938).
 - [5] L. Landau, *J. Phys. U.S.S.R.* **5**, 71 (1941).
 - [6] D. R. Tilley and J. Tilley, *Superfluidity and Superconductivity*, 3rd ed. (Institute of Physics Publishing, Bristol, 1990).
 - [7] R. J. Donnelly, *Quantized Vortices in Helium II*, edited by A. M. Goldman, P. V. E. McClintock, and M. Springfield (Cambridge University Press, Cambridge, England, 1991).
 - [8] W. Vinen and J. Niemela, *J. Low Temp. Phys.* **128**, 167 (2002).
 - [9] W. P. Halperin, *Progress in Low Temperature Physics, Vol. 16*, edited by M. Tsubota and W. Halperin (Elsevier, 2009).
 - [10] M. Tsubota, M. Kobayashi, and H. Takeuchi, *Phys Rep.* **522**, 191 (2013).
 - [11] C. F. Barenghi, L. Skrbek, and K. R. Sreenivasan, *Proc. Natl. Acad. Sci.* **111**, 4647 (2014).
 - [12] W. H. Zurek, *Nature (London)* **317**, 505 (1985).
 - [13] C. Bäuerle, Y. M. Bunkov, S. N. Fisher, H. Godfrin, and G. R. Pickett, *Nature* **382**, 332 (1996).
 - [14] Y. M. Bunkov, A. I. Golov, V. S. L'vov, A. Pomyalov, and I. Procaccia, *Phys. Rev. B* **90**, 024508 (2014).
 - [15] N. Andersson, K. Glampedakis, W. C. G. Ho, and C. M. Espinoza, *Phys. Rev. Lett.* **109**, 241103 (2012).
 - [16] D. Page, J. M. Lattimer, M. Prakash, and A. W. Steiner, *Stellar Superfluids*, edited by K. H. Bennemann and J. B. Ketterson, *Novel Superfluids Vol. 2* (Oxford Univ. Press, Oxford, 2014) Chap. 21.
 - [17] H. Yano, K. Ohyama, K. Obara, and O. Ishikawa, *J. Phys. Conf. Ser.* **969**, 012002 (2018).
 - [18] I. Matsumura, K. Ohyama, K. Sato, K. Obara, H. Yano, and O. Ishikawa, *J. Low Temp. Phys.* **196**, 204 (2019).
 - [19] D. V. Osborne, *Proc. R. Soc. A* **63**, 909 (1950).
 - [20] E. L. Andronikashvili and Y. G. Mamaladze, *Rev. Mod. Phys.* **38**, 567 (1966).
 - [21] K. W. Madison, F. Chevy, W. Wohlleben, and J. Dalibard, *Phys. Rev. Lett.* **84**, 806 (2000).
 - [22] K. W. Madison, F. Chevy, V. Bretin, and J. Dalibard, *Phys. Rev. Lett.* **86**, 4443 (2001).
 - [23] M. Tsubota, K. Kasamatsu, and M. Ueda, *Phys. Rev. A* **65**, 023603 (2002).
 - [24] K. Kasamatsu, M. Tsubota, and M. Ueda, *Phys. Rev. A* **67**, 033610 (2003).
 - [25] S. Z. Alamri, A. J. Youd, and C. F. Barenghi, *Phys. Rev. Lett.* **101**, 215302 (2008).
 - [26] K. W. Schwarz, *Phys. Rev. B* **31**, 5782 (1985).
 - [27] E. Varga, C. F. Barenghi, Y. A. Sergeev, and L. Skrbek, *EPJ Web of Conferences* **67**, 02124 (2014).
 - [28] G. A. Williams and R. E. Packard, *J. Low Temp. Phys.* **39**, 553 (1980).
 - [29] M. Tinkham, *Introduction to Superconductivity*, 2nd ed. (Dover Publications, Mineola, New York, 1996).
 - [30] (), see Supplemental Material 1 at ... for the VFM simulation in Region I.
 - [31] K. W. Schwarz, *Phys. Rev. Lett.* **64**, 1130 (1990).
 - [32] (), see Supplemental Material 2 at ... for the VFM simulation in Region II.
 - [33] H. von Helmholtz, *Phil. Mag.* **36**, 337 (1868).
 - [34] L. Kelvin, *Phil. Mag.* **42**, 362 (1871).
 - [35] R. Blaauwgeers, V. Eltsov, G. Eska, A. Finne, R. Haley, M. Krusius, J. Ruohio, L. Skrbek, and G. E. Volovik, *Phys. Rev. Lett.* **89**, 155301 (2002).
 - [36] (), see Supplemental Material 3 at ... for the VPM simulation in Region II.
 - [37] S. Yui, M. Tsubota, and H. Kobayashi, *Phys. Rev. Lett.* **120**, 155301 (2018).
 - [38] L. Birerale, D. Khomenko, V. S. L'vov, A. Pomyalov, I. Procaccia, and G. Sahoo, *Phys. Rev. B* **100**, 134515 (2019).
 - [39] S. Yui, H. Kobayashi, M. Tsubota, and W. Guo, *Phys. Rev. Lett.* **124**, 155301 (2020).
 - [40] L. Galantucci, A. W. Baggaley, C. F. Barenghi, and G. Krstulovic, *Eur. Phys. J. Plus* **135**, 547 (2020).
 - [41] M. Tsubota, T. Araki, and W. Vinen, *Physica B* **329-333** (2002).
 - [42] S. K. Nemirovskii, *Phys. Rev. B* **81**, 064512 (2010).
 - [43] A. Pomyalov, *Phys. Rev. B* **101**, 134515 (2020).
 - [44] (), the friction force \mathbf{f} on a vertical vortex filament that moves with \mathbf{v}_L , the velocity in the laboratory frame, per unit length is expressed as $\mathbf{f} = \gamma_0(\mathbf{v}_n - \mathbf{v}_L) + \gamma'_0 \mathbf{s}' \times (\mathbf{v}_n - \mathbf{v}_L)$. The relation between this friction parameter γ_0 and the mutual friction parameters, α and α' , discussed in

Eq. (2) is given as

$$\gamma_0 = \frac{\rho_n \rho_s}{2\rho} \kappa \frac{\alpha}{(1 - \alpha' \rho_n / 2\rho)^2 + \alpha^2 \rho_n^2 / 4\rho^2}$$

and

$$\gamma'_0 = \frac{\rho_n \rho_s}{2\rho} \kappa \frac{\alpha^2 \rho_n / 2\rho - \alpha' (1 - \alpha' \rho_n / 2\rho)}{(1 - \alpha' \rho_n / 2\rho)^2 + \alpha^2 \rho_n^2 / 4\rho^2}$$

[7, 46].

[45] (), see Supplemental Material 4 at ... for the VFM simulation for the vortex bundle diffusion.

[46] C. F. Barenghi, R. J. Donnelly, and Vinen, J. Low Temp. Phys. **52**, 189 (1983).